Abundance of cavity-free polaritonic states in resonant materials and nanostructures

(article starts on next page)

Abundance of cavity-free polaritonic states in resonant materials and nanostructures

Adriana Canales, Denis G. Baranov, Tomasz J. Antosiewicz, and Timur Shegai

COLLECTIONS

Paper published as part of the special topic on Polariton Chemistry: Molecules in Cavities and Plasmonic MediaPOM2020

View Online

Export Citation

CrossMark

ARTICLES YOU MAY BE INTERESTED IN

Molecular polaritons for controlling chemistry with quantum optics
The Journal of Chemical Physics **152**, 100902 (2020); https://doi.org/10.1063/1.5136320

Single vs double anti-crossing in the strong coupling between surface plasmons and molecular excitons
The Journal of Chemical Physics **154**, 024704 (2021); https://doi.org/10.1063/5.0037864

Improving the quality factors of plasmonic silver cavities for strong coupling with quantum emitters
The Journal of Chemical Physics **154**, 014703 (2021); https://doi.org/10.1063/5.0034739
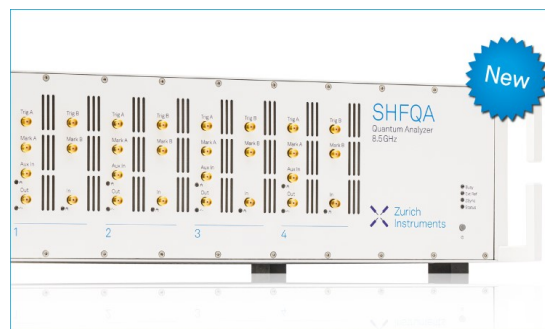
154, 024701

Abundance of cavity-free polaritonic states in resonant materials and nanostructures

View Online   Export Citation   CrossMark

Adriana Canales,[1] (iD) Denis G. Baranov,[1,2] Tomasz J. Antosiewicz,[1,3] (iD) and Timur Shegai[1,a)] (iD)

AFFILIATIONS

[1] Department of Physics, Chalmers University of Technology, 412 96 Göteborg, Sweden
[2] Center for Photonics and 2D Materials, Moscow Institute of Physics and Technology, Dolgoprudny 141700, Russia
[3] Faculty of Physics, University of Warsaw, Pasteura 5, 02-093 Warsaw, Poland

Note: This paper is part of the JCP Special Topic on Polariton Chemistry: Molecules in Cavities and Plasmonic Media.
[a)] Author to whom correspondence should be addressed: timurs@chalmers.se

ABSTRACT

Strong coupling between various kinds of material excitations and optical modes has recently shown potential to modify chemical reaction rates in both excited and ground states. The ground-state modification in chemical reaction rates has usually been reported by coupling a vibrational mode of an organic molecule to the vacuum field of an external optical cavity, such as a planar Fabry–Pérot microcavity made of two metallic mirrors. However, using an external cavity to form polaritonic states might (i) limit the scope of possible applications of such systems and (ii) might be unnecessary. Here, we highlight the possibility of using optical modes sustained by materials themselves to *self-couple* to their own electronic or vibrational resonances. By tracing the roots of the corresponding dispersion relations in the complex frequency plane, we show that electronic and vibrational polaritons are natural eigenstates of bulk and nanostructured resonant materials that require no external cavity. Several concrete examples such as a slab of the excitonic material and a spherical water droplet in vacuum are shown to reach the regime of such cavity-free self-strong coupling. The abundance of cavity-free polaritons in simple and natural structures points at their relevance and potential practical importance for the emerging field of polaritonic chemistry, exciton transport, and modified material properties.

I. INTRODUCTION

Strong coupling is a distinct regime of light–matter interactions realized when resonant optical modes and material excitations (electronic, vibrational, etc.) exchange energy faster than they lose it to the environment. This fast energy exchange gives rise to new quasiparticles: *polaritons*.[1,2]

Following the achievement of strong coupling, fundamental questions have arisen, such as whether polaritonic states could influence material and chemical properties.[3,4] The possibility of affecting chemical reactions in the excited state (i.e., photochemistry) seems to be quite well understood today. Several experimental studies show that strong coupling can affect photo-chemical processes,[5–7] and these results are essentially in agreement with

theoretical descriptions.[8–14] Thermally activated ground-state chemical reactions in the vibrational strong coupling (VSC) regime seem to be more controversial. In this case, just a few experimental reports exist,[15–18] and there is far less conclusive agreement with theory.[19–26]

An example of this controversy is given by common intuition, by stating that ground-state chemical reactions are local, i.e., the chemistry at position A does not depend on any far-away position B. Nevertheless, recent experimental studies[15–18] suggest that such a local approximation to the chemistry might not always hold. Contemporary empirical observations[3,4,27] indicate that the chemistry can be affected by resonant, collective, and non-local variables. For example, the reaction probability at a specific position depends on the far away presence (or absence) of metallic mirrors

forming a Fabry–Pérot (FP) cavity. Specifically, it depends on the set of resonant optical modes that the mirrors form. This set of resonant optical modes and its relevance to chemistry are especially important, since they distinguish polaritonic chemistry from other common non-local but non-resonant contributions, such as screening, electrostatic, and solvent polarity effects.[28–30] Moreover, while standard chemical theory states that the reaction rate depends on the concentration of molecules, concentration-dependent collective Rabi splitting influences the rate further by modifying the energy levels. Although this train of thought is heavily debated in the community, mainly due to a lack of theoretical understanding of the recent experimental observations, we believe that the potential of this new research frontier is quite high. Of course, further experiments and theoretical developments are needed to clarify this and other subtle issues.

Without trying to resolve the discrepancy of the ground-state chemistry in the VSC regime at this point, here, we are willing to focus on another potentially relevant issue. The so far experimentally reported observations of chemistry modifications under VSC exclusively use FP cavities comprised of two metallic mirrors.[15–18] Then, a natural question is if the role of the mirrors in these experiments is only to confine electromagnetic modes in order to form polaritons or if it goes beyond that. It is thus highly important to discuss the concept of "cavity" in the strong coupling regime and understand its relevance to polaritonic chemistry.

Traditionally, one requires an external cavity to reach strong coupling, such as a FP cavity, a plasmonic nanocavity, or a

photonic crystal cavity, schematically visualized in Fig. 1(a). Assuming that the role of the cavity is solely to confine the optical field, we argue that using external cavities may limit the scope of potential applications, as such cavities are impractical.[31] There also exist a number of the so-called "open" cavities, which might be more accessible and useful,[1,2,6] but also require an external object to provide the optical mode confinement. Here, we show that to achieve strong coupling, the cavity does not need to be external. Instead, electronic or vibrational excitations in bulk or nanostructured materials can *self-couple* to an optical mode sustained by its own geometry, as illustrated in Fig. 1(b). We consider a generic medium with a Lorentz dielectric function, motivated by the fact that optical properties of most materials can be modeled as such.

It is well known that objects with a refractive index different from their surrounding can sustain localized optical eigenmodes.[32] The characteristics of the modes depend on the geometry and refractive indices of the involved objects and its surroundings. If such an optical resonance is found in proximity to the material resonance, these optical and material resonances can hybridize and, provided that the oscillator strength of the transition is high, give rise to polaritons. The Rabi splitting of such self-hybridized polaritons can approach (but cannot exceed) the so-called bulk polariton splitting, which is a function of oscillator strength only and does not depend on parameters of the cavity. Such self-coupled or cavity-free polaritons have been realized in many relevant systems, such as slabs of hexagonal boron nitride

(a) Traditional polaritons: separate cavity mode
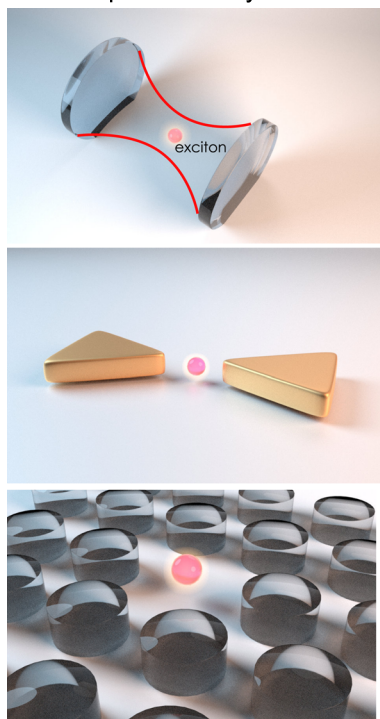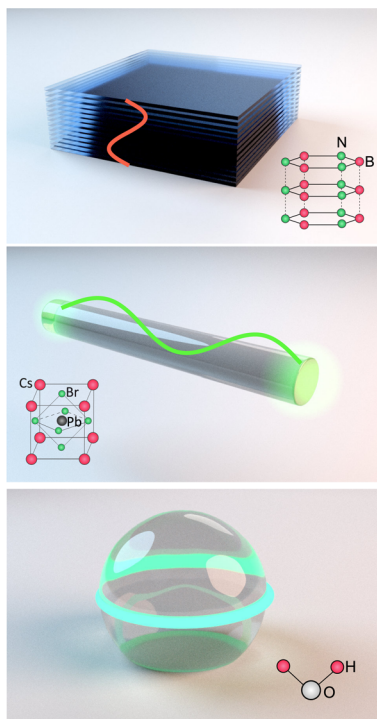
(b) Self-hybridized polaritons

FIG. 1. (a) Examples of architectures for traditional polaritons based on a separate cavity mode provided by a Fabry–Pérot resonator, a plasmonic resonator, or a photonic crystal cavity. (b) Examples of self-hybridized polaritons based on slabs, long nanorods, and spheres made of resonant (excitonic/Lorentzian) materials.

(hBN), transition metal dichalcogenides, perovskites, and plasmonic nanoparticles.[33–40] However, their relevance for the polaritonic chemistry and modified material properties has not risen in the community.

Originally, the problem of material resonance from the quantum optical light–matter coupling perspective has been solved by Hopfield in his seminal work in 1958.[41] Hopfield considered a three-dimensional (3D) continuous semiconductor and modeled it using a quantum coupled harmonic oscillator model but did not consider materials shaped into a specific object(s), which can sustain a set of discrete well-defined electromagnetic modes.

As we will show here, cavity-free polaritons are found in a great variety of structures, ranging from bulk materials to spherical microdroplets [Fig. 1(b)]. The sole existence and apparent abundance of such cavity-free polaritons indicate their applicability in polaritonic chemistry and, more generally, in any polariton-induced modifications of material properties.[30]

II. REVISITING STANDARD CAVITY-EMITTER POLARITONS

We start by revisiting the standard light–matter interaction Hamiltonian in Hopfield's formulation.[41] This formulation is essentially a coupled harmonic oscillator problem approached from the quantum optical perspective. We note that this is not exactly the same model as the famous Jaynes–Cummings or quantum Rabi models, which deal with two-level quantum emitters (QEs) coupled to a cavity mode. However, within the weak excitation regime, this formulation is sufficiently appropriate even for QEs and even more so within the scope of this study, since we utilize a macroscopic Lorentz-resonant description of matter.

The full Hopfield Hamiltonian for a cavity mode oscillating at a frequency ω_c interacting at a rate g with a material transition at a frequency ω_0, written in the Coulomb gauge and including the diamagnetic term, reads

$$\hat{H} = \hbar\omega_0\hat{b}^\dagger\hat{b} + \hbar\omega_c\hat{a}^\dagger\hat{a} + \hbar g(\hat{a}^\dagger + \hat{a})(\hat{b}^\dagger + \hat{b}) + \frac{\hbar g^2}{\omega_0}(\hat{a}^\dagger + \hat{a})^2, \quad (1)$$

where $\hat{b}$ and $\hat{a}$ are the annihilation operators of the material transition and the cavity mode, respectively, and g is the coupling constant.[42] Two eigenvalues (resonant transitions) of this Hamiltonian are given by

$$\omega_\pm = \frac{\sqrt{\omega_c^2 + 4g^2\omega_c/\omega_0 + \omega_0^2 \pm \sqrt{(\omega_c^2 + 4g^2\omega_c/\omega_0 + \omega_0^2)^2 - 4\omega_c^2\omega_0^2}}}{\sqrt{2}}. \quad (2)$$

With the material oscillators homogeneously occupying the cavity mode volume V, the coupling strength $g = \mu\sqrt{\rho V/3}\mathscr{E}_{vac}\omega_0/\omega_c$ (the factor 1/3 accounts for their isotropic orientation). Thus, the coupling strength depends on the transition dipole moment of the material transition, μ, and the volume density of these dipoles (oscillators), ρ, as well as the vacuum electric field of the cavity, $\mathscr{E}_{vac} = \sqrt{\hbar\omega_c/2\varepsilon_\infty\varepsilon_0 V}$. When the coupling strength is large enough (with respect to the losses, which are neglected in the above description for simplicity), two polaritons with different energies

[Eq. (2)] are formed, which has been explained in great detail before.[2,43]

The two main ingredients for achieving strong coupling are (i) an optical cavity with a large quality factor (Q) and a small mode volume (V) and (ii) an electronic (or vibrational) transition with a high transition dipole moment.[2] Following these suggestions, there has been extensive research to obtain the best optical cavities, ranging from high-finesse FP cavities composed of distributed Bragg reflector (DBR) mirrors to plasmonic nanocavities. Many of these cavities are covered by Baranov et al.[2] and some are depicted in Fig. 1(a).

In the examples above, we see that a stand-alone cavity is important for realizing the standard cavity-quantum electrodynamics (QED) scenario. That is the case of a single-QE strongly coupled to an external optical cavity. Such a scenario is challenging to realize with the cavity-free approach because a single QE problem cannot be treated in terms of a macroscopic Lorentz dielectric function even with the Hopfield Hamiltonian, as we do below, but instead requires a true cavity-QED approach, which we do not focus on here (these approaches are extensively covered in the literature[1,44]).

III. SELF-HYBRIDIZED POLARITONS

An optical mode is a concept that is not limited to the optical resonators and cavities discussed above. An optical mode is a solution of the source-free Maxwell equations in a given geometry. Thus, a cavity can be made of any material, including the material that makes up the relevant electronic or vibrational transitions themselves. These are precisely the scenarios we focus on in Secs. III A–III D.

A. 3D case: Bulk polaritons

Let us start by revisiting bulk polaritons, that is, hybrid light–matter states of an unbounded dielectric medium homogeneously filled with resonant transitions. This situation has been described by Hopfield in the celebrated 1958 paper[41] (see also the work of Mills and Burstein[45]). Instead of a localized eigenmode of a cavity, the photonic modes in this scenario are represented by plane waves propagating in the unbounded dielectric medium with permittivity ε_∞. Those waves have a continuous spectrum $\omega = kc/n$, with k being the vacuum wave vector, c being the speed of light, and $n = \sqrt{\varepsilon_\infty}$ being the refractive index of the medium.

In the classical electromagnetic formalism, an isotropic resonant medium can be described by a Lorentzian permittivity,

$$\varepsilon(\omega) = \varepsilon_\infty + f\frac{\omega_P^2}{\omega_0^2 - \omega^2 - i\gamma\omega}, \quad (3)$$

with $\omega_P = \sqrt{\rho e^2/3\varepsilon_0 m}$ being the plasma frequency, where ρ is the volume density of oscillators and 1/3 accounts for their isotropic orientation, e and m are the electron charge and mass, respectively, ω_0 and γ are the resonance frequency and linewidth, and f is the oscillator strength. The latter is expressed via the microscopic parameters of the medium as $f = 2\frac{m\omega_0}{e^2\hbar}|\mu|^2$, where μ is the transition dipole moment of the material oscillator (see Sec. VI). For simplicity, in

Eq. (3) and throughout this study (except for the case of hBN), we deal with only one resonance with an isotropic random orientation of transitions. Extensions of this simplified model can describe more complicated cases, e.g., by including several Lorentz resonances and anisotropy.

Bulk polaritons correspond to roots of the dispersion equation,

$$kc - \omega\sqrt{\varepsilon(\omega)} = 0. \tag{4}$$

One can look for solutions of this equation either with complex ω and real k or complex k and real ω. These two types are both appropriate solutions of Maxwell's equations but suited for different purposes.[46] We are interested in complex-ω solutions of the dispersion equation, since they better reflect the transient decay of hybrid light–matter states of the coupled system.

Quantitative characteristics of the problem, such as the vacuum Rabi splitting and the magnitude of the polaritonic gap, can be obtained from the Hamiltonian formulation, which neglects exciton dissipation.[41] Following the standard procedure of quantizing the electromagnetic field in free space, let us consider a quantization box of volume L^3 with periodic boundary conditions.[47] The vacuum electric field of a photon with frequency ω_c reads $\mathscr{E}_{vac} = \sqrt{\hbar\omega_c/2\varepsilon_\infty\varepsilon_0 L^3}$. Recalling the expression for the oscillator strength f and plasma frequency ω_P of a Lorentz medium, we express the resulting coupling strength as $g_C = (\omega_P/2)\sqrt{f\omega_0/\varepsilon_\infty\omega_c}$. The vacuum Rabi splitting (with zero losses) is then obtained as the difference between the two polariton energies [Eq. (2)] for the zero-detuned photon ($\omega_c = \omega_0$),

$$\Omega_R = \sqrt{2g^2 + \omega_0^2 + 2g\sqrt{g^2 + \omega_0^2}} - \sqrt{2g^2 + \omega_0^2 - 2g\sqrt{g^2 + \omega_0^2}} = 2g_0, \tag{5}$$

where $g_0 = (\omega_P/2)\sqrt{f/\varepsilon_\infty}$ is the zero-detuning coupling strength.

The upper edge of the polariton gap is obtained by calculating the upper polariton energy in the limit $k = 0$ and is $\widetilde{\omega}_0 = \sqrt{\omega_0^2 + 4g_0^2}$, where $\widetilde{\omega}_0$ is the re-normalized resonance frequency. The lower edge of the gap is found by calculating the lower polariton energy in the limit $k \to \infty$, and is exactly the uncoupled exciton energy ω_0. This results in the polaritonic gap

$$\Delta_{pol} = \sqrt{\omega_0^2 + 4g_0^2} - \omega_0, \tag{6}$$

which simplifies to $\Delta_{pol} \approx 2g_0^2/\omega_0$ under the assumption of $4g_0^2/\omega_0^2 \ll 1$, which holds in the standard strong coupling regime. In the formalism of dielectric permittivity, this bandgap can be interpreted as the Reststrahlen band of the material: the domain of energies wherein the real part of the permittivity becomes negative, thus forbidding propagation of plane waves.[41]

The presence of losses in the dielectric formalism makes the eigenfrequencies complex and changes their dispersion; the original Hopfield model of bulk polaritons does not include any dissipation channels. Subsequent works extended Hopfield's model to account for exciton decay by considering coupling between them and a continuum bath of harmonic oscillators.[48] Such a model predicts that bulk polaritons appear if and only if the condition

$$f\omega_P^2 > \varepsilon_\infty\gamma^2/4 \tag{7}$$

holds. It is easy to see that this condition is equivalent to $(\omega_P/2)\sqrt{f/\varepsilon_\infty} = g_0 > \gamma/4$, which is the strong coupling criterion in the standard Jaynes–Cummings model with a lossless cavity mode.[48,49] Thus, by knowing the parameters of the material resonance in Eq. (3), it is possible to estimate the bulk coupling strength at zero detuning g_0 and compare it to $\gamma/4$ in order to conclude whether or not this specific material supports bulk polaritons.

Figures 2(a)–2(c) show the dispersion (k vs real part of ω) of bulk polaritons [obtained as roots of Eq. (4)] of a medium described by the permittivity in Eq. (3), with typical values for TDBC J-aggregates ($\omega_0 = 2.11$ eV, $\gamma = 0.1$ eV, and $\varepsilon_\infty = 2.15$)[50] and varying oscillator strengths. First, for $f\omega_P^2 = 0.0045$ eV^2, corresponding to a strongly diluted J-aggregate, we observe the mode attraction typical for the weak coupling regime [Fig. 2(a)]. In this regime, the energies of the eigenmodes of the medium slightly deviate from the bare values, but their dispersions cross near the zero detuning region.

For a larger oscillator strength $f\omega_P^2 = 0.445$ eV^2 (see the work of Balasubrahmaniyam *et al.*),[50] one can clearly see an anticrossing between the two polaritonic modes, with the vacuum Rabi splitting around 455 meV. We calculate the vacuum Rabi splitting as the energy separation along the real frequency axis between polaritonic modes obtained at a zero detuning between the electronic resonance of the material and the bare cavity mode (in turn, obtained by setting $f = 0$). This choice corresponds to nearly 50%/50% exciton/photon polariton wave-function amplitudes, and we use this definition throughout the text. On the same plot, we also show dispersion of complex-k/real-ω solutions (in a red solid line) found simply as $k = \sqrt{\varepsilon(\omega)}\omega/c$. The two solutions coincide away from the resonance but differ in the vicinity of ω_0. While the two branches of complex-ω solutions are disconnected, the two branches of the complex-k solutions are connected by the region of anomalous dispersion.

For even larger oscillator strength, $f\omega_P^2 = 3.116$ eV^2 (we note here that this value is unrealistically large for J-aggregates and we give it here only for the sake of theoretical argument; there may be other material systems where such oscillator strengths are feasible), the dispersion shows a larger vacuum Rabi splitting of about 1.2 eV and also displays a polaritonic gap—a region of frequencies with no propagating modes within it, shown in Fig. 2(c).[41,44,51] The corresponding complex-k solutions, at the same time, span over the whole range of frequencies but become highly damped within the polariton gap by acquiring a large imaginary part of the wave vector k (see Fig. S1).

In addition to the anticrossing in the k–ω plane, it is instructive to inspect trajectories of the roots of the dispersion in Eq. (4) in the complex-ω plane. Figures 2(d)–2(f) show trajectories of the complex frequency roots for the three cases of weak, strong, and ultrastrong coupling. In the weak coupling, $f\omega_P^2 < \varepsilon_\infty(\gamma/2)^2$, the "photonic" root of the equation crosses the exciton position and acquires a small imaginary component in the zero detuning region, while the "excitonic" root (the one originating at the complex exciton frequency, marked with a yellow star in Fig. 2) moves along a finite curve around $\omega_0 - i\gamma/2$. However, in the strong and ultrastrong
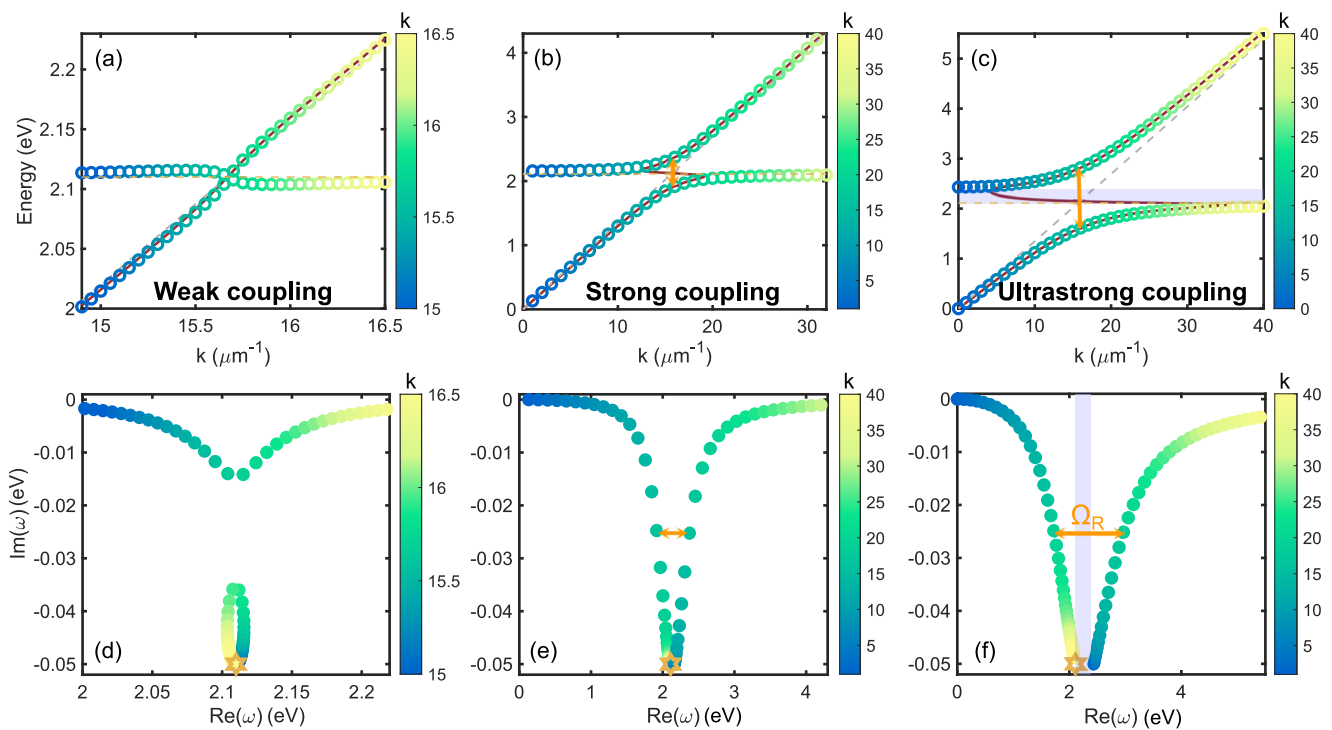
FIG. 2. Bulk polaritons. The upper panels show the dispersion of bulk J-aggregate polaritons considering the complex-k and real-ω solutions in a red solid line and the complex-ω and real-k eigenmodes in circles for (a) weak coupling with $f\omega_P^2 = 0.0045$ eV^2, (b) strong coupling with $f\omega_P^2 = 0.445$ eV^2, and (c) ultrastrong coupling with $f\omega_P^2 = 3.116$ eV^2, which displays a polaritonic gap shaded in blue. The dashed lines denote the dispersion of the uncoupled exciton (yellow at 2.11 eV) and the light dispersion in vacuum (gray). The lower panels show the trajectories of the complex frequency roots for the same values in the three regimes: (d) weak, (e) strong, and (f) ultrastrong coupling. The location of the uncoupled exciton ($\omega_0 - i\gamma/2$) is marked as a yellow star. The Rabi splitting is marked by orange arrows. The color bar represents the value of k in μm^{-1}.

coupling regimes, the low-energy solution terminates exactly at the exciton energy, while the upper solution originates on the other side of the polaritonic gap [Figs. 2(e) and 2(f)].

In closing this part, we want to emphasize that bulk polaritonic states and the whole anticrossing picture exist in an optically large piece of a resonant material without any external cavity.

B. 2D case: Polaritons in Lorentz slabs

The examples given above clearly illustrate that a large (compared to the resonance wavelength) unstructured excitonic or phononic material already possesses polaritonic modes, provided that the oscillator strength of the material exceeds the threshold value. Reducing the dimension of the system (by breaking the translational invariance in one, two, or all three dimensions) does not break this picture: the reduced system still possesses optical modes (either complex-frequency resonant states or real-frequency guided modes) that couple with the material resonance.

Let us first reduce the bulk material in one dimension (along the z-axis to be specific) and consider a slab with a Lorentzian permittivity $\varepsilon(\omega)$ in vacuum. The eigenmodes of this system can be quantified by the (real) in-plane momentum k_x, k_y.[52] In the absence of the

material resonance, the modes above the light line are FP resonances with complex frequencies (not to be confused with real-frequency leaky modes);[53] and the modes below the light line are proper waveguide modes with real frequencies.[54] Upon inclusion of the material resonance, it couples to modes both below and above the light line.

Figure 3(a) presents the eigenfrequency spectrum of TE-polarized eigenmodes of a 200 nm thick J-aggregate slab with $f\omega_P^2 = 0.445$ eV^2 obtained as roots of the characteristic Eq. (13) (see Sec. VI). Such a J-aggregate was also analyzed in Figs. 2(b) and 2(e) corresponding to the bulk strong coupling case. It shows the real part of eigenfrequencies vs the in-plane momentum k_x on top of the reflection spectrum calculated above the light line. Eigenfrequencies of the slab are found numerically as poles of the reflection coefficient in the lower half plane of the complex frequency (see Sec. VI). Remarkably, spectral positions of FP modes above the light line do not always coincide with reflection dips, as shown in Fig. 3(a) for polaritonic modes and in Fig. S3 for bare modes ($f = 0$) of a dielectric slab. This behavior comes from non-resonant contributions of other poles of the dielectric slab, particularly the fundamental waveguide mode present at any k_x.[52] This mismatch should be always kept in mind in the analysis of experimental or simulated spectra of coupled exciton–polariton systems.
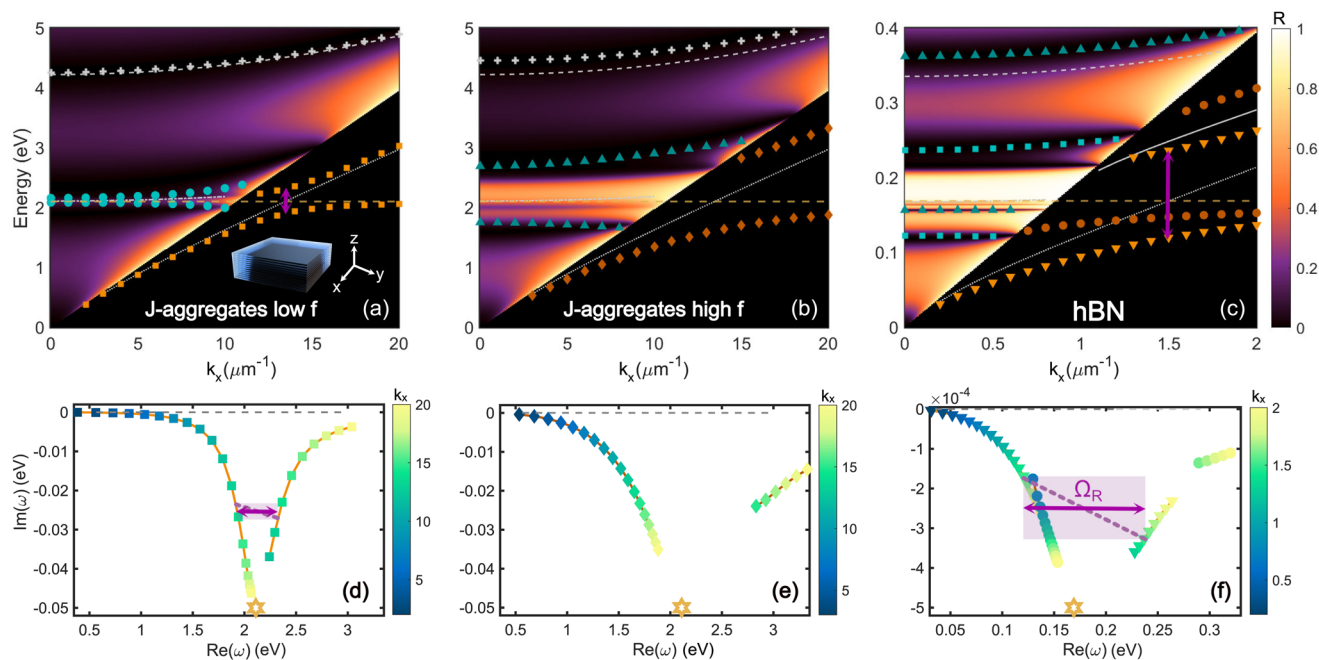
FIG. 3. Polaritons in dielectric slabs. The upper panels show dispersion of the Fabry–Pérot (FP) and guided modes over the reflection spectra of TE polarized light of (a) a 200 nm thick J-aggregate slab with $f\omega_P^2 = 0.445$ eV^2 and (b) with $f\omega_P^2 = 3.116$ eV^2 and (c) a 1.75 μm thick slab of hBN with $f\omega_P^2 = 0.064$ eV^2. The lower panels show the trajectories, in the complex-ω plane, of the polaritons resulting from the first guided mode of the slab (TE$_1$) hybridizing with the resonance in the same materials as above: (d) J-aggregates with low f—squares, (e) J-aggregates with high f—diamonds, and (f) hBN—down-pointing triangles for hybridization with TE$_1$ and circles for that with TE$_2$. The color bar represents k_x. The Rabi splitting with TE$_1$ is marked with a purple arrow. The uncoupled modes are shown in dashed and dotted lines.

The 200 nm thick slab with $f\omega_P^2 = 0.445$ eV^2 does not show any noticeable splitting above the light line [circles in Fig. 3(a)]: the coupling strength is not sufficient to overcome the large radiative decay of the FP mode. Below the light line, however, there is a clear anti-crossing between the exciton and the TE$_1$ waveguide mode with a magnitude of Rabi splitting around 420 meV, which is smaller than the 455 meV of bulk Rabi splitting previously mentioned.

TE-polarized eigenmodes of a 200 nm thick J-aggregate slab with a higher oscillator strength $f\omega_P^2 = 3.16$ eV^2 demonstrate anticrossing both below and above the light line [Fig. 3(b)]. This J-aggregate was analyzed in Figs. 2(c) and 2(f) and corresponds to the bulk ultrastrong coupling case. In this case, the magnitude of the Rabi splitting (purple arrows in the rest of the panels) cannot be obtained because the upper polariton has a cut-off given by the light line and the corresponding guided eigenmode does not exist.

Next, we demonstrate self-hybridized polaritons in another practically relevant system: a slab of hexagonal boron nitride (hBN). hBN exhibits two prominent vibrational modes at 169 meV and 95 meV, respectively.[55] We focus on TE-polarized modes, which couple only with the in-plane vibrations of hBN at 169 meV. The in-plane permittivity component of hBN can be described by a single Lorentz term with $\varepsilon_\infty = 4.45$, $f\omega_P^2 = 0.064$ eV^2, and $\gamma = 1$ meV, which approximates the experimental data in the relevant spectral range [Fig. S1(g)].[55]

Figure 3(c) shows eigenfrequencies of TE-polarized eigenmodes of a 1.75 μm thick hBN slab. Clearly, there are anticrossings both below (circles and down-pointing triangles) and above (squares and triangles) the light line, thanks to the large oscillator strength of hBN's vibrational transition. For the same reason, we also observe the lower polariton branch of the second FP mode above the light line, shown in blue triangles, and lower polariton of the TE$_2$ waveguide mode below the light line (shown in orange circles). The Rabi splitting of the TE$_1$ waveguide mode, which occurs at about $k_x = 1.5$ μm^{-1}, reaches a value of $\approx$116 meV, which is also below the bulk Rabi splitting, $2g_0 \approx 120$ meV. Remarkably, below the light line, polaritons formed by interaction of the fundamental modes TE$_1$ and TE$_2$ with the phonon show pronounced anticrossing, even though the TE$_2$ mode dispersion in a dielectric slab without the exciton does not approach the exciton energy [see Fig. 3(c)].

This behavior becomes more evident when we look at trajectories of the eigenmodes' poles of the slab in the complex-ω plane. It turns out, that even for a vanishingly small oscillator strength $f\omega_P^2$, there are countably many poles in an arbitrarily small vicinity of the complex exciton frequency $\omega_0 - i\gamma/2$ [see Fig. S4(b)], where the Lorentz permittivity $\varepsilon(\omega)$ has a simple pole [shown in Fig. S4(c)].[56,57] Each of these poles represents an eigenmode of the Lorentzian slab: either a radiative mode or a localized waveguide mode, depending on the position of the pole frequency with respect to the complex plane cut.

The origin of this cluster of poles can be appreciated by considering the Lorentzian permittivity ε at complex frequencies [Fig. S4(c)]. One can clearly see that just below the complex exciton frequency, $\omega_0 - i\gamma/2$, the permittivity takes arbitrarily large values, thus, in theory, allowing for the existence of higher-order FP and waveguide modes that are otherwise inaccessible at real frequencies, where the permittivity is bounded by $|\varepsilon(\omega)| \leq \varepsilon_\infty + f\omega_P^2/\gamma\omega_0$.

Because these poles are located so close, they usually merge into a single spectral feature in real-frequency spectral responses, often attributed to "uncoupled molecules."[58,59] In fact, as the complex frequency plane reveals, this feature stems from a whole new multitude of eigenmodes located in the small vicinity of the complex exciton energy (Fig. S4). Of course, only a finite number of these eigenmodes are physical, since the permittivity becomes highly non-local and loses its physical meaning as soon as the wavelength inside the material $\lambda/\mathrm{Re}(\sqrt{\varepsilon(\omega)})$ at complex ω approaches the microscopic length scale of the medium near the pole.

Complex-plane trajectories also clearly reveal the Rabi splitting. Above the light-line, trajectories of the eigenmodes are limited by the low frequency cutoff on the one side and by the light line on the other side and, for this reason, are difficult to interpret (Fig. S5). Below the light line, however, only the upper polariton branches are bounded by the light line on the low energy side [Fig. 3(d)] and the resulting trajectories are very similar to those for bulk polaritons [see Fig. 2(e)]. Qualitatively similar pictures of anticrossing in the $\omega - k_x$ space and in the complex-ω plane are found for TM-polarized eigenmodes (Fig. S6).

Since the waveguide modes of a dielectric slab have virtually infinite lifetime in contrast to radiative FP modes, anticrossing below the light line appears at a much smaller oscillator strength.

For an electrically thin film, we can establish an approximate analytical criterion of strong coupling for waveguide modes. Assuming an electrically thin dielectric film without the Lorentzian transition ($k_0 L \sqrt{\varepsilon_\infty} \ll 1$, where L is the thickness of the film), the dispersion of the TE_1 waveguide mode is approximately

$$k_x \approx k_0(1 + \delta k), \quad \delta k = (k_0 L)^2 (\varepsilon_\infty - 1)/8, \qquad (8)$$

with δk being a small parameter for a thin film (see Sec. VI). The vacuum field of the bare TE waveguide mode at the center of the dielectric slab can be estimated as $\mathscr{E}_{vac} = \sqrt{\hbar\omega_c/2\varepsilon_0 a^2 W}$, where $W = 1/\Im(k_{z,1}) \approx \frac{1}{k_0\sqrt{2\delta k}}$ is the waveguide mode's effective width. Multiplying the vacuum field by the square root of the number of oscillators $\sqrt{\rho a^2 L}$ in the volume $a^2 L$ and the dipole moment μ, we find the coupling strength (at zero detuning, $\omega_c = \omega_0$ and $k_0 = \omega_0/c$),

$$g = \frac{\omega_P}{2}(k_0 L)\sqrt{\frac{f\sqrt{\varepsilon_\infty - 1}}{2}}. \qquad (9)$$

Comparing the above g to $\gamma/4$, we find the threshold oscillator strength required for anticrossing below the light line in a dielectric film,

$$f\omega_P^2 > \frac{\gamma^2}{2(k_0 L)^2\sqrt{\varepsilon_\infty - 1}}. \qquad (10)$$

This condition may help estimate the minimal thickness L of an excitonic film required for the emergence of polaritonic modes below the light line for a given oscillator strength.
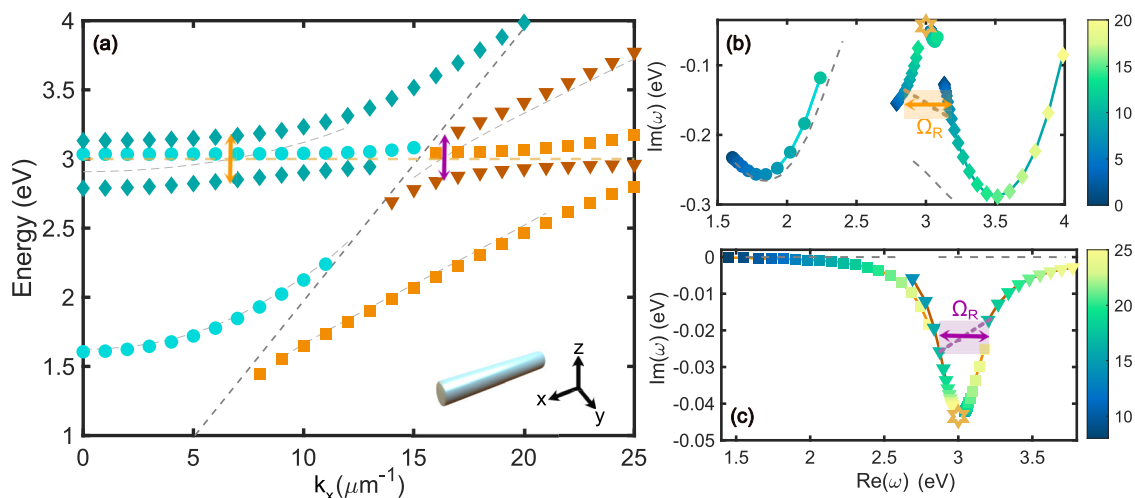
FIG. 4. Polaritons in infinite circular cylinders. (a) Dispersion of the polaritons given with the TM radiating modes of the $CsPbCl_3$ cylinder, with a radius of 250 nm, above (first mode in circles and second mode in diamonds) and waveguide modes below the light line (first mode in squares and second in down-pointing triangles). Trajectories of the hybrid modes with (b) radiating and (c) waveguide modes in the complex-ω plane. The color bar shows the value of k_x and the colored arrows show the Rabi splitting above (orange) and below (purple) the light line. The uncoupled optical modes are shown by dashed lines.

C. 1D case: Polaritons in long circular cylinders

By reducing the system in one more dimension (say, along the y-axis), we arrive at one possessing translational invariance only in a single direction (along the x-axis). Thanks to this symmetry, eigenmodes of the one-dimensional system are characterized by a real-valued momentum k_x. Similar to the 2D case, eigenmodes with $k_x > \omega/c$ are guided modes with real frequencies; eigenmodes with $k_x < \omega/c$ are radiating resonances with complex frequencies.

For simplicity, let us focus on 1D systems with a circular cross section. The states with $k_x = 0$ (normal-incidence resonances of the cylinder) are classified by their polarization state (TE or TM) and the azimuthal number m.[60] Eigenmodes with $k_x \neq 0$ split into TE and TM-polarized solutions only for $m = 0$ (the monopole harmonic).[61] For $m > 0$, TE and TM polarizations couple, giving rise to hybrid modes named EHnm and HEnm. The HE11 mode (the dipole mode) is the only mode of a circular cylindrical dielectric waveguide not having a cutoff[61] [see down-pointing traingles in Figs. S7(a) and S7(c)].

As a practical example, we demonstrate self-hybridized polaritons in infinite circular cylinders of a perovskite CsPbCl₃. This material is described by a Lorentz permittivity with $\varepsilon_\infty = 3.7$, $\omega_0 = 3$ eV, $\gamma = 87$ meV, and $f\omega_P^2 = 0.54$ eV² that approximates the

experimental data[37] [see Fig. S1(a)]. Polaritons and polaritonic emission in long whiskers made of perovskites of various families have been demonstrated in a number of works.[36,62]

Figure 4 presents the eigenfrequency spectrum of TM-polarized monopole ($m = 0$) eigenmodes [obtained as roots of the characteristic Eq. (16); see Sec. VI] for the CsPbCl₃ infinitely long circular cylinder with a radius of 250 nm. The resulting spectrum clearly shows anticrossing above the light line (involving the second order radiating mode) and below the light line (involving the TM₀,₁ waveguide mode). The anticrossing below the light line features a Rabi splitting of about 312 meV, which compares to bulk Rabi splitting of CsPbCl₃ of 382 meV. Complex-ω trajectories of eigenfrequencies exhibit a familiar behavior with upward frequency pulling to the real axis above the light line and downward pulling below the light line [Figs. 4(b) and 4(c)]. Qualitatively similar eigenfrequencies are obtained for TE-polarized monopole modes (Fig. S8) and for the dipole TEM modes (Fig. S7).

D. 0D case: Polaritons in spheres

Finally, if we reduce the system in one more dimension, we end up with a compact scatterer supporting a discreet spectrum
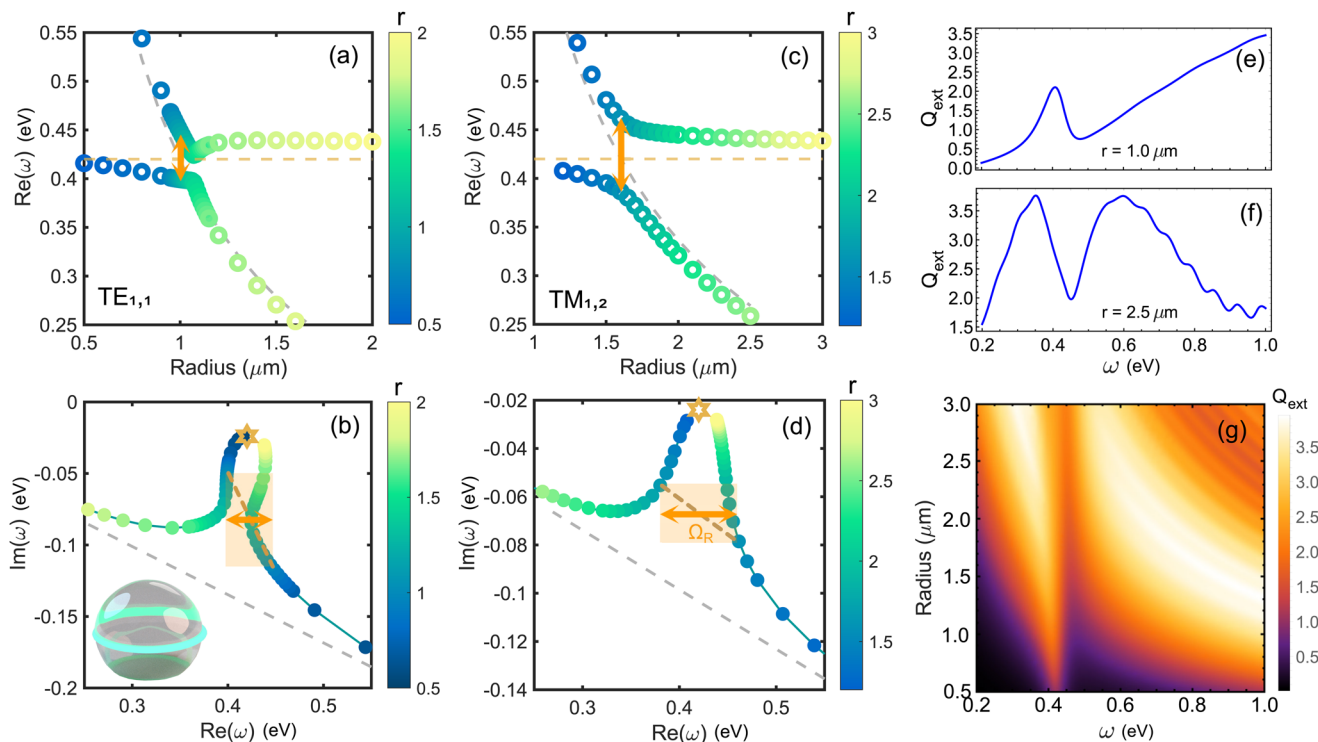

FIG. 5. Polaritons in water spheres. The upper left panels show eigenfrequency dependence on the radius of a water sphere for (a) TE₁,₁ and (c) TM₁,₂ modes. The lower left panels show the trajectories of the complex $-\omega$ roots for the same modes (b) TE₁,₁ and (d) TM₁,₂ by varying the radius (shown in the colormap). The poles at zero detuning are noted in the trajectories as the vertices of the orange rectangle joined by the dashed line. The Rabi splitting is the width of such a rectangle in Re(ω). The right panels show the extinction efficiency, Q_{ext}, for water droplets of radius (e) $r = 1$ μm, which is too small to show strong coupling, and (f) $r = 2.5$ μm, which is large enough to show the splitting in Q_{ext}. Both plots are included in (g) where a range of sizes is covered.

of localized eigenmodes.[63,64] Because of the lack of translational invariance in any direction, all eigenmodes of the scatterer are complex-frequency radiating solutions.[65]

To keep the analysis simple, we consider the most symmetric compact scatterer: a sphere whose eigenmodes are the well-known Mie resonances.[66] These resonances split into TE- and TM-polarized modes, which are further classified by the angular index l and the radial number N. $l = 1$ modes are usually referred to as the dipole ones, $l = 2$ is referred to as the quadrupole ones, and so on. A detailed description of whispering gallery exciton–polaritons in GaAs spheres has been presented by Platts et al.[33] Because of the lack of translational invariance, the anticrossing in spheres cannot be seen by scanning the eigenmode's momentum k. Instead, one usually varies the radius of the sphere, which causes the eigenmodes to move in the ω-space.

As a practically interesting example of self-hybridized polaritons in spheres, we consider liquid water droplets. Liquid water has a strong vibrational resonance around 420 meV with the oscillator strength of $f\omega_P^2 = 0.035$ eV^2.[67] Therefore, one may naturally expect formation of vibrational polaritons in Mie resonant micrometer-sized water droplets. We describe water by a Lorentz permittivity with $\varepsilon_\infty = 1.75$, $\omega_0 = 0.42$ eV, $\gamma = 0.048$ eV, and $f\omega_P^2 = 0.035$ eV^2 that approximates the experimental data [see Fig. S1(d)].[67]

Figure 5(a) shows eigenfrequencies of TE$_{1,1}$ (magnetic dipole) eigenmodes of a water sphere as a function of its radius r. The trajectory of the TE$_{1,1}$ eigenmode (the first index indicates the angular number of the mode l and the second index stands for the radial number of the mode N) shows a clear anticrossing with a magnitude of about 30 meV for a sphere with $r \approx 1.1$ μm [Fig. 5(c)]. This value is significantly lower than the corresponding bulk Rabi splitting for water $\omega_P\sqrt{f/\varepsilon_\infty} \approx 100$ meV due to high radiative loss of

the TE$_{1,1}$ mode. The small value of the Rabi splitting in this case is also manifested in the shape of the dispersion curves, similar to the exceptional point (EP) regime with the square root dependence of eigenenergies on the perturbation parameter (such as the radius).[68]

We find that 1.1 μm is the smallest radius for which polaritonic modes appear in water spheres. Although the TM$_{1,1}$ (electric dipole) eigenmode of smaller $r \approx 600$ nm spheres with $\varepsilon_\infty = 1.75$ matches the vibrational resonance position, it has a much lower Q-factor, which prevents strong coupling in spheres of this size (Fig. S9).

Nevertheless, the TM$_{1,2}$ mode of $r \approx 1.7$ μm spheres does demonstrate a clear anticrossing with the water vibration [Figs. 5(b) and 5(d)], producing a Rabi splitting of about 70 meV, which approaches the bulk splitting of 100 meV. Complex-ω trajectories in both cases reveal the characteristic eigenfrequency pulling to the real axis [Figs. 5(c) and 5(d)] originating from large radiative losses of the bare optical mode compared to the exciton linewidth. With the increase in radius of the sphere, new eigenmodes corresponding to higher orbital and radial numbers (also having a higher Q-factor) will match the vibrational resonance position and show additional anticrossings and polaritonic modes.

We further investigate how the attainable Rabi splitting in water spheres depends on the eigenmode polarization and the orbital number. Figure 6(a) shows the Rabi splitting for TE and TM eigenmodes as a function of the orbital number l. One can see that the Rabi splitting of TE modes systematically exceeds that of TM modes for all orbital numbers, but both gradually approach the bulk water splitting, $2g_0$, which for water is ~100 meV (see Table S1).

We also illustrate how polaritonic modes of micrometer-sized water spheres manifest themselves in extinction spectra at real

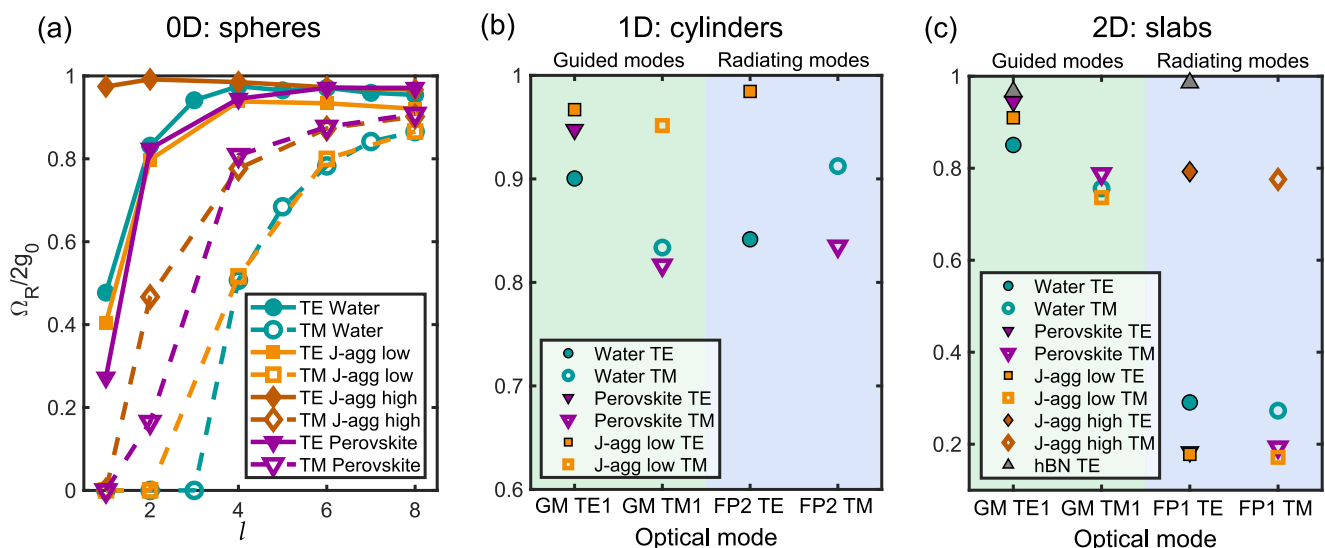FIG. 6. Limit of Rabi splitting. Normalized Rabi splitting for all the materials as a function of the optical mode for all the geometries discussed above: (a) spheres, (b) infinite cylinders, and (c) slabs. The guided modes are shaded in green, and the radiating modes are shaded in blue. The dimensions of the structures and the values of $2g_0$ are found in Sec. V of the supplementary material.

frequencies. For droplets of 1 μm radius, no splitting is observed in extinction, as shown in Fig. 5(e). On the other hand, Fig. 5(f) shows observable splitting for a 2.5 μm radius droplet. The false color plot in Fig. 5(g) clearly demonstrates an avoided crossing in the extinction efficiency of a sphere as function of its radius r, $Q_{ext} = \sigma_{ext}/\pi r^2$ (see Sec. VI), which is the quantity most easily accessible with optical techniques from a macroscopic ensemble of microspheres. An important note to make is that the anticrossing in extinction spectra, being the sum of all the eigenmodes, significantly overestimates the splitting. Absorption and scattering efficiencies, whose sum constitutes extinction, calculated in a wider range of water droplet parameters, are shown in Fig. S9.

Coincidentally, micrometer-sized droplets of liquid water that support vibrational self-polaritons are quite ubiquitous in nature. For example, a common size of water droplets in fogs, mists, clouds, or steams falls exactly into the range of 1 μm–10 μm that is needed for the formation of vibrational Mie self-polaritons. Due to surface tension, these droplets adopt a spherical geometry, thus forming an ideal natural platform for the observation of vibrational self-polaritons in strong and even ultrastrong coupling regimes. Note that the bulk polariton splitting of liquid water falls into the vibrational ultrastrong coupling regime, since $g_0^{H_2O} \approx 0.05$ eV and $g_0^{H_2O}/\omega_0^{H_2O} = \eta_0^{H_2O} \approx 0.12 > 0.1$, which satisfies the ultrastrong coupling criterion.[26]

IV. DISCUSSION

A. Critical size for the cavity-free polariton formation

In this section, we turn our attention to the apparent fact that nanostructures supporting cavity-free polaritons have a certain critical size below which no polaritonic behavior is observed. For example, water spheres below $\approx$1 μm in radius will not support polaritons. Such size-limiting behavior is, of course, not universal to water and should be observed in all Lorentz materials [e.g., $r_{min} \approx 98$ nm for perovskite and $\approx$180 nm for J-aggregates in Fig. 6(a)]. Neither is it exclusive to the spherical geometry. For dielectric slabs, where the fundamental waveguide modes do not have a cutoff, the physical reason for the critical size is the delocalization of the electric field of the mode and a resulting weak coupling strength. For circular cylinders (also their monopole modes) and spheres, the size bound stems from the fact that the fundamental eigenmodes of electrically small systems are far blue-detuned with respect to the material transition resonance, the case in which efficient hybridization is not possible. Finally, we would like to mention that in the opposite case of exceedingly large 0D–2D objects, the result is trivial and reduces to the bulk case, which has no critical upper limit.

From the material-science perspective, the existence of the critical size suggests that the polaritonic behavior and hence modified material properties are supported only within a certain size range, given by the material resonant properties, its surrounding(s), and its shape.

It is also worth noting that, from the computational point of view, the particles of about the critical size, although they are on the order of several tens to several hundreds of nanometers, contain a large number of oscillators (atoms or molecules).

Thus, it is challenging to self-consistently capture these collective cavity-free polaritons using atomistic methods, such as density functional theory,[23,69] due to their high computational cost.

B. The limit of Rabi splitting

The diversity of realizations of strong coupling, both using cavities (Fig. 1) and in the cavity-free format (Figs. 2–5), raises a question about the limit of g and Ω_R that one can observe using Lorentz materials. A particularly important question is whether it is the material or the cavity that plays the decisive role in this limit.

To shed light on this issue, we compare the bulk polariton coupling strength to the other realizations for the specific Lorentz material considered above (Fig. 6). From the presented data, it appears that the lossless bulk polariton splitting, $2g_0 = \omega_P\sqrt{f/\varepsilon_\infty}$ (see Table S1 for the values for each material), indeed establishes an ultimate limit on vacuum Rabi splitting achievable with a given Lorentz material with *any* cavity mode. Indeed, a cavity of mode volume V supporting a localized eigenmode can host only as many as $N = V\rho$ transitions. Assuming that they all couple to the mode with an identical coupling strength, which is certainly an overestimation, the resulting Rabi splitting is seen to be bound from top by the bulk polariton coupling. The lossless bulk polariton splitting is, in turn, limited from above by setting $f = \varepsilon_\infty = 1$, which gives $\Omega_R^{max} = 2g_0^{max} = \omega_P$. Thus, the maximum bulk polariton splitting is principally limited from above by the volume density of oscillators—ρ (also a combination of natural constants).

It is also instructive to consider the maximum ratio between the coupling strength and the resonance frequency $\eta^{max} = g_0^{max}/\omega_0 = \omega_P/2\omega_0$. This ratio plays an important role when the coupling strength approaches the transition frequency. Specifically, when $\eta > 0.1$, one usually distinguishes the ultrastrong coupling (USC) regime, while when $\eta > 1$, one distinguishes the deep strong coupling (DSC) regime. Taking in mind the principal limits of the coupling strength, the parameter η is seen to be intrinsically related to the ratio of plasma and resonant frequencies in Lorentz materials. This ratio can be both below one and significantly above one (in principle, unbound) depending on the material. However, one should keep in mind that in the limit of DSC, the light and matter components of the polaritonic states actually *decouple*, presenting nearly uncoupled optical mode and material excitation as the eigenstates of the system.[70] This decoupling can be seen as the result of the screening by the diamagnetic term. In order to maintain equal cavity/matter fractions, one would have to tune the matter transition in resonance with the renormalized cavity mode. The same decoupling occurs in the dipole gauge, where the matter resonance experiences a de-polarization shift due to dipole–dipole interaction of the electronic subsystem.[71] In fact, considering the ratio between the coupling constant and the renormalized resonance frequency $\eta = g_0/\widetilde{\omega}_0 = g_0/\sqrt{\omega_0^2 + 4g_0^2}$, one can see that the latter is principally bound by $\eta \le 1/2$.[72] This hard limit indicates impossibility of reaching DSC with Lorentz media (if normalization is performed with respect to the renormalized frequency).

Since the Rabi splitting is limited from above by the bulk polariton coupling strength, having a separate cavity at best allows confining polaritons in space but does not increase the coupling strength due to the above limitation. As we showed above, the optical mode confinement can be attained without a separate cavity in the first place, with the exciton (or phonon) material itself playing the role of a confining resonator.

The bulk polariton splitting limit may serve as practical guidance for the selection of the material platform in strong coupling experiments. This limit is the function of the material only and does not depend on the nature of the cavity. For any practical realization of strong coupling, the observed Rabi splitting can only approach that of the bulk, $2g_0 = \omega_P\sqrt{f/\varepsilon_\infty}$, an estimation of which is straightforward (requires no complicated simulation). Thus, a material with a high enough oscillator strength will naturally support polaritonic eigenstates in all studied 0D–3D regimes.

V. CONCLUSION

In summary, we have shown that polaritonic states are natural and ubiquitous to bulk materials and nanostructures that can be described by a generic Lorentz resonance(s). Such polaritons are universally encountered in systems that do not involve any stand-alone cavities or metallic mirrors. In these cavity-free systems, boundaries of the Lorentz medium play the role of the mirrors that allow formation of well-defined optical modes, which, in turn, couple to the resonant transition. We demonstrated such cavity-free polaritonic states in 3D-bulk materials, 2D-slabs, 1D-cylinders, and 0D-spheres. Concrete examples of real material systems including spherical water droplets, perovskite nanocylinders, and slabs of J-aggregates and hBN were provided.

These findings might have important implications for the recently observed modification of material and chemical properties seen in electronic and vibrational strongly coupled systems. In particular, from the classical electromagnetism point of view, as well as the Hopfield Hamiltonian treatment, the cavity-free polaritons are *no* different from the more standard microcavity polaritons containing dense molecular layers. Thus, all observations relevant to the cavity polaritons could just also be applicable to the cavity-free polaritons presented here, provided that it is indeed the polaritonic nature of those modes that is responsible for chemistry and material science modifications (other reasons such as the usage of highly polarizable metallic mirrors as was done in nearly all experimental studies so far might also play a role[31]). However, in the cavity-free case, the exact polaritonic eigenmode picture depends on the size and shape of the resonant material and its environment. Thus, if we accept the hypothesis that polaritonic states themselves (not the presence of metallic mirrors) are able to modify material and chemical properties, then these material and chemical properties should be dependent on the size and shape of this material, in agreement with the cavity-free polaritonic eigenmode picture. Clearly, such a cavity-free approach to modified material properties is beneficial from the practical point of view, as many of these structures exist naturally and is thus trivial to fabricate. A common concrete example considered here are the water droplets (encountered in fogs, mists,

and clouds), which have a sharp cutoff below the radius of about 1 μm. Smaller water droplets will not support vibrational Mie self-polaritons and thus may experience different chemical properties in comparison to bigger droplets that support vibrational Mie self-polaritons and to bulk water that supports bulk vibrational polaritons. Similar consequences may apply to J-aggregates, hBN, etc., as well as to any Lorentz material with a high enough oscillator strength of the relevant (electronic or vibrational) transition. This reasoning applies also to polariton-assisted modification of other material-related properties. We look forward to experimental tests of these predictions.

VI. METHODS

A. Permittivity of bulk medium

The permittivity of a resonant medium containing electronic or vibrational transitions can be obtained by calculating the electric dipole polarizability of a single such transition and combining it with the volume density of homogeneously distributed transitions ρ in the medium.

The dipolar polarizability of a two-level system with the transition dipole moment μ in a weak external field can be written as

$$\hat{\alpha}_{\text{TLS}} = \hat{\mathbf{f}}\frac{e^2/\varepsilon_0 m}{\omega_0^2 - \omega^2 - i\gamma\omega}, \quad \hat{\mathbf{f}} = 2\frac{m\omega_0}{e^2\hbar}\mu \otimes \mu, \tag{11}$$

where $\hat{\mathbf{f}}$ is the transition's oscillator strength, m is the electron mass, e is the electron charge, and $\otimes$ is the outer product[73] (note ε_0 in the expression for polarizability, as required in SI units). Combining this with the volume density of the two-level systems ρ and assuming random orientation of transition dipole moments, one easily obtains the expression for the polarization density and permittivity of the medium,

$$\varepsilon = \varepsilon_\infty + f\frac{\omega_P^2}{\omega_0^2 - \omega^2 - i\gamma\omega}, \tag{12}$$

where ε_∞ is the non-resonant background permittivity, $\omega_P^2 = \rho e^2/(3\varepsilon_0 m)$ is the plasma frequency, and the factor $1/3$ accounts for random isotropic orientation of dipoles in the medium.

B. Eigenfrequencies of a slab

Eigenfrequencies of a planar slab of thickness L are found as poles of the reflection coefficient in the complex frequency plane. The reflection coefficient of a TE or TM polarized plane wave with the wavenumber $k_0 = \omega/c$ and in-plane momentum k_x reads

$$R_{\text{TE,TM}} = \frac{r_{\text{TE,TM}}(1 - e^{2ik_{z,2}L})}{1 - r_{\text{TE, TM}}^2 e^{2ik_{z,3}L}}, \tag{13}$$

where

$$r_{\text{TE}} = \frac{k_{z,1} - k_{z,2}}{k_{z,1} + k_{z,2}}, \quad r_{\text{TM}} = \frac{k_{z,1} - k_{z,2}/\varepsilon(\omega)}{k_{z,1} + k_{z,2}/\varepsilon(\omega)}, \tag{14}$$

with $k_{z,1} = \sqrt{k_0^2 - k_x^2}$ and $k_{z,2} = \sqrt{\varepsilon(\omega)k_0^2 - k_x^2}$ being the z-components of the wave vector in vacuum and dielectric, respectively.

$k_{z,1}$ has a branching point at $k_x = k_0$, and a cut needs to be made. The field of the eigenmode outside the slab is described by the phase factor $e^{\pm ik_{z,1}z}$, where the plus and minus sign is applied in the regions $z > L/2$ and $z < -L/2$ correspondingly. The radiating modes above the light line should have $\Re(k_{z,1}) > 0$, while proper waveguide modes have $\Im(k_{z,1}) > 0$. Therefore, we make the branch cut along the negative imaginary axis through $\omega = -i\infty$ and choose the Riemann sheet of the square root function such that $\Re(k_{z,1}) > 0$ above the light line and $\Im(k_{z,1}) > 0$ below the light line. This choice ensures that we find radiating eigenmodes and proper (localized) waveguide modes. Choosing another Riemann sheet of the square root in the definition of $k_{z,1}$ results in dispersion of improper (diverging) modes below the light line. The choice of sheet for $k_{z,2}$ is not important because the slab contains both waves with $\pm k_{z,2}$.

C. Dispersion of the TE_1 waveguide mode in a thin dielectric film

Dispersion of TE waveguide modes in a dielectric film is given by the roots of the characteristic equation $1 - r_{TE}^2 e^{2ik_{z,2}L} = 0$. This is a transcendental equation and, in a general case, cannot be solved analytically. However, in the case of an electrically thin film ($k_0 L\sqrt{\varepsilon_\infty} \ll 1$), the equation can be linearized and an approximate solution of the fundamental TE_1 mode can be found.

For an electrically thin film, dispersion of the TE_1 mode is sandwiched between the light line of the environment ($k_0 = \omega/c$) and that of the slab ($k = \sqrt{\varepsilon_\infty}\omega/c$) and follows very close to the environment light line; therefore, we can write the propagation constant of the guided mode as $k_x = k_0 + \delta k$, where $\delta k \ll k_0$. The z components of the wave vectors in the environment and in the slab can be expanded as follows:

$$k_{z,1} = \sqrt{k_0^2 - k_x^2} \approx i\sqrt{2k_0 \delta k},$$

$$k_{z,2} = \sqrt{\varepsilon k_0^2 - k_x^2} \approx k_0\sqrt{\varepsilon - 1}\left(1 - \frac{\delta k}{(\varepsilon - 1)k_0}\right).$$

Note that $k_{z,1}$ scales as $O(\sqrt{\delta k})$, whereas the leading correction to $k_{z,2}$ scales as $O(\delta k)$. The exponential phase factor can be expanded in a Taylor series $e^{2ik_{z,2}L} \approx 1 + 2ik_{z,2}L$. Plugging these expansions into the characteristic equation, we obtain

$$\left(\frac{k_{z,1} - k_{z,2}}{k_{z,1} + k_{z,2}}\right)^2 (1 + 2ik_{z,2}L) - 1 = 0,$$

$$i(k_{z,1}^2 - 2k_{z,1}k_{z,2} + k_{z,2}^2)L = 2k_{z,1}.$$

Keeping only the leading power $O(\sqrt{\delta k})$ of the k_x expansion and the constant term $O(1)$ in this equation, we find $\delta k = k_0^3 L^2(\varepsilon - 1)/8$, and the approximate dispersion relation of the TE_1, correspondingly, can be written as

$$k_x \approx k_0 + k_0^3 L^2 \frac{\varepsilon - 1}{8}. \tag{15}$$

D. Eigenfrequencies of a cylinder

TE (TM) modes of an infinitely long cylinder are defined as those having their electric (magnetic) field strictly perpendicular to the cylinder axis. Eigenfrequencies of TE01 and TM01 (monopole transverse electric and transverse magnetic, respectively) waveguide modes of an infinitely long circular cylinder of radius a are found as roots of the following characteristic equations:[60,61]

$$\frac{\varepsilon}{k_{\rho,2}} \frac{J_1'(k_{\rho,2}a)}{J_1(k_{\rho,2}a)} - \frac{1}{k_{\rho,1}} \frac{H_1'(k_{\rho,1}a)}{H_1(k_{\rho,1}a)} = 0, \quad \text{(TM)} \tag{16}$$

$$\frac{1}{k_{\rho,2}} \frac{J_1'(k_{\rho,2}a)}{J_1(k_{\rho,2}a)} - \frac{1}{k_{\rho,1}} \frac{H_1'(k_{\rho,1}a)}{H_1(k_{\rho,1}a)} = 0, \quad \text{(TE)} \tag{17}$$

where $J_1(z)$ and $H_1(z) = H_1^{(1)}(z)$ are Bessel and Hankel functions of the first kind, respectively, and $k_{\rho,1} = \sqrt{k_0^2 - k_x^2}$ and $k_{\rho,2} = \sqrt{\varepsilon(\omega)k_0^2 - k_x^2}$ are the radial wavenumber of the eigenmode in vacuum and dielectric, respectively.

The definition of $k_{\rho,1}$ requires a branch cut at $k_{\rho,1} = k_0$. Radial dependence of the eigenmode field outside the waveguide is given by the factor $H_1(k_{\rho,1}\rho)$. Therefore, making the branch cut going along the negative imaginary axis through $\omega = -i\infty$ and choosing the Riemann sheet yielding $\text{Re}(k_{\rho,1}) > 0$ above the light-line results in the spectrum of radiating eigenmodes and localized waveguide modes.[60]

Eigenfrequencies of the HE11 (dipole) mode are found as roots of the following characteristic equation:[61]

$$\left[\frac{1}{k_{\rho,2}} \frac{J_1'(k_{\rho,2}a)}{J_1(k_{\rho,2}a)} - \frac{1}{k_{\rho,1}} \frac{H_1'(k_{\rho,1}a)}{H_1(k_{\rho,1}a)}\right]\left[\frac{1}{k_{\rho,2}} \frac{J_1'(k_{\rho,2}a)}{J_1(k_{\rho,2}a)}\right.$$
$$\left. - \frac{1}{k_{\rho,1}} \frac{H_1'(k_{\rho,1}a)}{H_1(k_{\rho,1}a)}\right] = \left[\frac{k_x}{k_0} \frac{(\varepsilon - 1)k_0^2}{a^2 k_{\rho,1}^2 k_{\rho,2}^2}\right]^2. \quad \text{(HE11)}. \tag{18}$$

E. Eigenfrequencies of a sphere

TE (TM) modes of a sphere are defined as those having their electric (magnetic) field strictly perpendicular to the radial direction. Eigenfrequencies of TE and TM polarized modes with orbital number l are found as roots of the corresponding characteristic equations,

$$\psi_l(nx)\xi_l'(x) - n\xi_l(x)\psi_l'(nx) = 0, \quad \text{(TE)} \tag{19}$$

$$n\psi_l(nx)\xi_l'(x) - \xi_l(x)\psi_l'(nx) = 0. \quad \text{(TM)}. \tag{20}$$

Scattering coefficients a_n and b_n of the sphere of a sphere of radius a and permittivity $\varepsilon = n^2$ in vacuum in the basis of TE and TM polarized spherical harmonics are given by the classical Mie solution,[66]

$$a_n = \frac{n\psi_l(nx)\psi_l'(x) - \psi_l(x)\psi_l'(nx)}{n\psi_l(nx)\xi_l'(x) - \xi_l(x)\psi_l'(nx)}, \tag{21}$$

$$b_n = \frac{\psi_l(nx)\psi_l'(x) - n\psi_l(x)\psi_l'(nx)}{\psi_l(nx)\xi_l'(x) - n\xi_l(x)\psi_l'(nx)}, \tag{22}$$

where $x = k_0 a$, $\psi_l(x) = xj_l(x)$, and $\xi_l(x) = xh_l^{(1)}(x)$ are Ricatti–Bessel functions and $j_l(x)$ and $h_l^{(1)}(x)$ are spherical Bessel and Hankel functions of the first kind, respectively.

The extinction and scattering efficiencies of the sphere are given by the sum over all harmonics,[66]

$$Q_{ext} = \frac{2}{x^2} \sum_{n=1}^{\infty} (2n+1)\Re(a_n + b_n), \tag{23}$$

$$Q_{sca} = \frac{2}{x^2} \sum_{n=1}^{\infty} (2n+1)(|a_n|^2 + |b_n|^2). \tag{24}$$

SUPPLEMENTARY MATERIAL

See the supplementary material for the additional mode analysis, permittivities of the materials, and scattering and absorption spectra of water droplets calculated in a wider size range.

ACKNOWLEDGMENTS

DATA AVAILABILITY

The data that support the findings of this study are available from the corresponding author upon reasonable request.

REFERENCES

[1] P. Törmä and W. L. Barnes, "Strong coupling between surface plasmon polaritons and emitters: A review," Rep. Prog. Phys. **78**, 013901 (2014).

[2] D. G. Baranov, M. Wersäll, J. Cuadra, T. J. Antosiewicz, and T. Shegai, "Novel nanostructures and materials for strong light–matter interactions," ACS Photonics **5**, 24–42 (2018).

[3] T. W. Ebbesen, "Hybrid light–matter states in a molecular and material science perspective," Acc. Chem. Res. **49**, 2403–2412 (2016).

[4] J. Feist, J. Galego, and F. J. Garcia-Vidal, "Polaritonic chemistry with organic molecules," ACS Photonics **5**, 205–216 (2018).

[5] J. A. Hutchison, T. Schwartz, C. Genet, E. Devaux, and T. W. Ebbesen, "Modifying chemical landscapes by coupling to vacuum fields," Angew. Chem., Int. Ed. **51**, 1592–1596 (2012).

[6] B. Munkhbat, M. Wersäll, D. G. Baranov, T. J. Antosiewicz, and T. Shegai, "Suppression of photo-oxidation of organic chromophores by strong coupling to plasmonic nanoantennas," Sci. Adv. **4**, eaas9552 (2018).

[7] V. N. Peters, M. O. Faruk, J. Asane, R. Alexander, D. A. Peters, S. Prayakarao, S. Rout, and M. A. Noginov, "Effect of strong coupling on photodegradation of the semiconducting polymer P3HT," Optica **6**, 318–325 (2019).

[8] J. Galego, F. J. Garcia-Vidal, and J. Feist, "Many-molecule reaction triggered by a single photon in polaritonic chemistry," Phys. Rev. Lett. **119**, 136001 (2017).

[9] J. Galego, F. J. Garcia-Vidal, and J. Feist, "Suppressing photochemical reactions with quantized light fields," Nat. Commun. **7**, 13841 (2016).

[10] F. Herrera and F. C. Spano, "Cavity-controlled chemistry in molecular ensembles," Phys. Rev. Lett. **116**, 238301 (2016).

[11] R. F. Ribeiro, L. A. Martínez-Martínez, M. Du, J. Campos-Gonzalez-Angulo, and J. Yuen-Zhou, "Polariton chemistry: Controlling molecular dynamics with optical cavities," Chem. Sci. **9**, 6325–6339 (2018).

[12] J. Fregoni, G. Granucci, E. Coccia, M. Persico, and S. Corni, "Manipulating azobenzene photoisomerization through strong light–molecule coupling," Nat. Commun. **9**, 4688 (2018).

[13] S. Felicetti, J. Fregoni, T. Schnappinger, S. Reiter, R. de Vivie-Riedle, and J. Feist, "Photoprotecting uracil by coupling with lossy nanocavities," J. Phys. Chem. Lett. **11**, 8810–8818 (2020).

[14] N. Nefedkin, E. Andrianov, and A. Vinogradov, "The role of strong coupling in the process of photobleaching suppression," J. Phys. Chem. C **124**, 18234–18242 (2020).

[15] A. Thomas, J. George, A. Shalabney, M. Dryzhakov, S. J. Varma, J. Moran, T. Chervy, X. Zhong, E. Devaux, C. Genet et al., "Ground-state chemical reactivity under vibrational coupling to the vacuum electromagnetic field," Angew. Chem., Int. Ed. **55**, 11462–11466 (2016).

[16] A. Thomas, L. Lethuillier-Karl, K. Nagarajan, R. M. Vergauwe, J. George, T. Chervy, A. Shalabney, E. Devaux, C. Genet, J. Moran, and T. W. Ebbesen, "Tilting a ground-state reactivity landscape by vibrational strong coupling," Science **363**, 615–619 (2019).

[17] J. Lather, P. Bhatt, A. Thomas, T. W. Ebbesen, and J. George, "Cavity catalysis by cooperative vibrational strong coupling of reactant and solvent molecules," Angew. Chem., Int. Ed. **58**, 10635–10638 (2019).

[18] K. Hirai, R. Takeda, J. A. Hutchison, and H. Uji-i, "Modulation of Prins cyclization by vibrational strong coupling," Angew. Chem., Int. Ed. **132**, 5370–5373 (2020).

[19] J. Flick, M. Ruggenthaler, H. Appel, and A. Rubio, "Atoms and molecules in cavities, from weak to strong coupling in quantum-electrodynamics (QED) chemistry," Proc. Natl. Acad. Sci. U. S. A. **114**, 3026–3034 (2017).

[20] L. A. Martínez-Martínez, R. F. Ribeiro, J. Campos-González-Angulo, and J. Yuen-Zhou, "Can ultrastrong coupling change ground-state chemical reactions?," ACS Photonics **5**, 167–176 (2018).

[21] J. Galego, C. Climent, F. J. Garcia-Vidal, and J. Feist, "Cavity Casimir-Polder forces and their effects in ground-state chemical reactivity," Phys. Rev. X **9**, 021057 (2019).

[22] J. A. Campos-Gonzalez-Angulo, R. F. Ribeiro, and J. Yuen-Zhou, "Resonant catalysis of thermally activated chemical reactions with vibrational polaritons," Nat. Commun. **10**, 4685 (2019).

[23] C. Schäfer, M. Ruggenthaler, H. Appel, and A. Rubio, "Modification of excitation and charge transfer in cavity quantum-electrodynamical chemistry," Proc. Natl. Acad. Sci. U. S. A. **116**, 4883–4892 (2019).

[24] J. A. Campos-Gonzalez-Angulo and J. Yuen-Zhou, "Polaritonic normal modes in transition state theory," J. Chem. Phys. **152**, 161101 (2020).

[25] V. P. Zhdanov, "Vacuum field in a cavity, light-mediated vibrational coupling, and chemical reactivity," Chem. Phys. **535**, 110767 (2020).

[26] T. E. Li, J. E. Subotnik, and A. Nitzan, "Cavity molecular dynamics simulations of liquid water under vibrational ultrastrong coupling," Proc. Natl. Acad. Sci. U. S. A. **117**, 18324–18331 (2020).

[27] J. Yuen-Zhou and V. M. Menon, "Polariton chemistry: Thinking inside the (photon) box," Proc. Natl. Acad. Sci. U. S. A. **116**, 5214–5216 (2019).

[28] V. Peters, T. Tumkur, G. Zhu, and M. Noginov, "Control of a chemical reaction (photodegradation of the P3HT polymer) with nonlocal dielectric environments," Sci. Rep. **5**, 14620 (2015).

[29] K. J. Lee, Y. Xiao, J. H. Woo, E. Kim, D. Kreher, A.-J. Attias, F. Mathevet, J.-C. Ribierre, J. W. Wu, and P. André, "Charge-transfer dynamics and nonlocal dielectric permittivity tuned with metamaterial structures as solvent analogues," Nat. Mater. **16**, 722–729 (2017).

[30] V. N. Peters, S. Prayakarao, S. R. Koutsares, C. E. Bonner, and M. A. Noginov, "Control of physical and chemical processes with nonlocal metal–dielectric environments," ACS Photonics **6**, 3039–3056 (2019).

[31] An alternative assumption is that a two-metallic-mirrors cavity significantly modifies the density of electromagnetic states inside the cavity, as compared to the free space, by both increasing the density at resonance(s) and decreasing it

away from resonance(s) over a very broad spectral range, in a spirit similar to a Faraday cage, which may affect chemistry and other material-related properties in both resonant and non-resonant ways (making this scenario different from the self-coupled polaritons discussed below). Such an assumption may be realistic and we cannot exclude it at this point. However, in what follows, we focus on the analysis of polaritonic eigenmodes of the system in the assumption that these polaritonic modes are somehow important for chemistry, as was suggested in the recent literature.[15]

[32] J. D. Jackson, *Classical Electrodynamics*, 3rd ed. (John Wiley and Sons, Inc., New York, 1999).

[33] C. E. Platts, M. A. Kaliteevski, S. Brand, R. A. Abram, I. V. Iorsh, and A. V. Kavokin, "Whispering-gallery exciton polaritons in submicron spheres," Phys. Rev. B **79**, 245322 (2009).

[34] Z. Pirzadeh, T. Pakizeh, V. Miljkovic, C. Langhammer, and A. Dmitriev, "Plasmon–interband coupling in nickel nanoantennas," ACS Photonics **1**, 158–162 (2014).

[35] P.-Z. Chen, Y.-X. Weng, L.-Y. Niu, Y.-Z. Chen, L.-Z. Wu, C.-H. Tung, and Q.-Z. Yang, "Light-harvesting systems based on organic nanocrystals to mimic chlorosomes," Angew. Chem., Int. Ed. **55**, 2759–2763 (2016).

[36] S. Zhang, Q. Shang, W. Du, J. Shi, Z. Wu, Y. Mi, J. Chen, F. Liu, Y. Li, M. Liu, Q. Zhang, and X. Liu, "Strong exciton–photon coupling in hybrid inorganic–organic perovskite micro/nanowires," Adv. Opt. Mater. **6**, 1701032 (2018).

[37] E. Y. Tiguntseva, D. G. Baranov, A. P. Pushkarev, B. Munkhbat, F. Komissarenko, M. Franckevičius, A. A. Zakhidov, T. Shegai, Y. S. Kivshar, and S. V. Makarov, "Tunable hybrid Fano resonances in halide perovskite nanoparticles," Nano Lett. **18**, 5522–5529 (2018).

[38] B. Munkhbat, D. G. Baranov, M. Stührenberg, M. Wersäll, A. Bisht, and T. Shegai, "Self-hybridized exciton-polaritons in multilayers of transition metal dichalcogenides for efficient light absorption," ACS Photonics **6**, 139–147 (2019).

[39] R. Verre, D. G. Baranov, B. Munkhbat, J. Cuadra, M. Käll, and T. Shegai, "Transition metal dichalcogenide nanodisks as high-index dielectric Mie nanoresonators," Nat. Nanotechnol. **14**, 679–684 (2019).

[40] Y.-C. Chen, B. Song, A. J. Leggett, P. Ao, and X. Zhu, "Resonant confinement of an excitonic polariton and ultraefficient light harvest in artificial photosynthesis," Phys. Rev. Lett. **122**, 257402 (2019).

[41] J. Hopfield, "Theory of the contribution of excitons to the complex dielectric constant of crystals," Phys. Rev. **112**, 1555 (1958).

[42] D. G. Baranov, B. Munkhbat, E. Zhukova, A. Bisht, A. Canales, B. Rousseaux, G. Johansson, T. J. Antosiewicz, and T. Shegai, "Ultrastrong coupling between nanoparticle plasmons and cavity photons at ambient conditions," Nat. Commun. **11**, 2715 (2020).

[43] G. Khitrova, H. Gibbs, M. Kira, S. W. Koch, and A. Scherer, "Vacuum Rabi splitting in semiconductors," Nat. Phys. **2**, 81–90 (2006).

[44] A. Frisk Kockum, A. Miranowicz, S. De Liberato, S. Savasta, and F. Nori, "Ultrastrong coupling between light and matter," Nat. Rev. Phys. **1**, 19–40 (2019).

[45] D. L. Mills and E. Burstein, "Polaritons: The electromagnetic modes of media," Rep. Prog. Phys. **37**, 817–926 (1974).

[46] J. G. N. Rahmeier, V. Tiukuvaara, and S. Gupta, "Complex eigenmodes and eigenfrequencies in electromagnetics," arXiv:2005.05491 (2020).

[47] L. Landau and E. Lifshitz, *Course of Theoretical Physics*, 3rd ed., Quantum Mechanics, Non-Relativistic Theory Vol. 3 (Pergamon Press, 1977).

[48] B. Huttner and S. M. Barnett, "Quantization of the electromagnetic field in dielectrics," Phys. Rev. A **46**, 4306–4322 (1992).

[49] S. De Liberato, "Virtual photons in the ground state of a dissipative system," Nat. Commun. **8**, 1465 (2017).

[50] M. Balasubrahmaniyam, C. Genet, and T. Schwartz, "Coupling and decoupling of polaritonic states in multimode cavities," arXiv:2005.03527 (2020).

[51] P. Forn-Díaz, L. Lamata, E. Rico, J. Kono, and E. Solano, "Ultrastrong coupling regimes of light-matter interaction," Rev. Mod. Phys. **91**, 025005 (2019).

[52] L. J. Armitage, M. B. Doost, W. Langbein, and E. A. Muljarov, "Resonant-state expansion applied to planar waveguides," Phys. Rev. A **89**, 053832 (2014).

[53] P. Lalanne, W. Yan, K. Vynck, C. Sauvan, and J.-P. Hugonin, "Light interaction with photonic and plasmonic resonances," Laser Photonics Rev. **12**, 1700113 (2018).

[54] Strictly speaking, radiating complex-frequency eigenmodes of the slab extend below the light-line, and only indirectly connect to the waveguide modes via a branch of the improper mode dispersion. However, this effect is very subtle and can be ignored in the present analysis.

[55] J. D. Caldwell, L. Lindsay, V. Giannini, I. Vurgaftman, T. L. Reinecke, S. A. Maier, and O. J. Glembocki, "Low-loss, infrared and terahertz nanophotonics using surface phonon polaritons," Nanophotonics **4**, 44–68 (2015).

[56] W. Broer and B. J. Hoenders, "Natural modes and resonances in a dispersive stratified N-layer medium," J. Phys. A: Math. Theor. **42**, 245207 (2009).

[57] E. A. Muljarov and W. Langbein, "Resonant-state expansion of dispersive open optical systems: Creating gold from sand," Phys. Rev. B **93**, 075417 (2016).

[58] T. J. Antosiewicz, S. P. Apell, and T. Shegai, "Plasmon–exciton interactions in a core–shell geometry: From enhanced absorption to strong coupling," ACS Photonics **1**, 454–463 (2014).

[59] P. Fauché, C. Gebhardt, M. Sukharev, and R. A. Vallée, "Plasmonic opals: Observation of a collective molecular exciton mode beyond the strong coupling," Sci. Rep. **7**, 4107 (2017).

[60] M. B. Doost, W. Langbein, and E. A. Muljarov, "Resonant state expansion applied to two-dimensional open optical systems," Phys. Rev. A **87**, 043827 (2013).

[61] A. Ishimaru, *Electromagnetic Wave Propagation, Radiation, and Scattering: From Fundamentals to Applications* (John Wiley & Sons, 2017).

[62] T. J. Evans, A. Schlaus, Y. Fu, X. Zhong, T. L. Atallah, M. S. Spencer, L. E. Brus, S. Jin, and X.-Y. Zhu, "Continuous-wave lasing in cesium lead bromide perovskite nanowires," Adv. Opt. Mater. **6**, 1700982 (2018).

[63] P. R. Conwell, P. W. Barber, and C. K. Rushforth, "Resonant spectra of dielectric spheres," J. Opt. Soc. Am. A **1**, 62–67 (1984).

[64] M. B. Doost, W. Langbein, and E. A. Muljarov, "Resonant-state expansion applied to three-dimensional open optical systems," Phys. Rev. A **90**, 013834 (2014).

[65] Except for the rare case of embedded eigenstates, which can occur in 0D systems only if it contains $\varepsilon = 0$ materials.

[66] C. F. Bohren and D. R. Huffman, *Absorption and Scattering of Light by Small Particles* (Wiley, 2004), p. 530.

[67] D. J. Segelstein, "The complex refractive index of water," Ph.D. thesis, University of Missouri–Kansas City, 1981.

[68] K. Özdemir, S. Rotter, F. Nori, and L. Yang, "Parity–time symmetry and exceptional points in photonics," Nat. Mater. **18**, 783–798 (2019).

[69] T. P. Rossi, T. Shegai, P. Erhart, and T. J. Antosiewicz, "Strong plasmon-molecule coupling at the nanoscale revealed by first-principles modeling," Nat. Commun. **10**, 3336 (2019).

[70] S. De Liberato, "Light-matter decoupling in the deep strong coupling regime: The breakdown of the Purcell effect," Phys. Rev. Lett. **112**, 016401 (2014).

[71] Y. Todorov and C. Sirtori, "Intersubband polaritons in the electrical dipole gauge," Phys. Rev. B **85**, 045304 (2012); arXiv:1212.5140.

[72] A. Vasanelli, Y. Todorov, and C. Sirtori, "Ultra-strong light–matter coupling and superradiance using dense electron gases," C. R. Phys. **17**, 861–873 (2016).

[73] L. Novotny and B. Hecht, *Principles of Nano-Optics* (Cambridge University Press, 2012).